

## Planetary Geology

### Figure Captions



**Figure 36.1** Barringer Crater in northern Arizona.

This impact crater was created 50,000 years ago by an iron meteorite measuring 50 m across. The meteorite struck the ground at 40,000 km/hr, producing a blast equivalent to a 20-megaton hydrogen bomb. The crater itself is 1.2 km across and 200 m deep. (*Meteor Crater Enterprises, Arizona*)

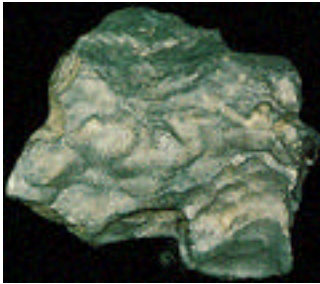


**Figure 36.2** Stony meteorite.

Most meteorites that strike Earth are stony. Stony meteorites look much like ordinary rocks, except some (like this one) are covered with a dark crust. This particular meteorite fell in Texas. (*Ronald A. Oriti*)



**Figure 36.3** Details of a lunar crater.

This photograph was taken from lunar orbit by astronauts in 1969. This is a typical view of the Moon's heavily cratered far side. The large crater in the center is approximately 80 km in diameter. Note the crater's central peak and the many tiny craters that pockmark the lunar surface. (*NASA*)



**Figure 36.4** Mare Imbrium and surrounding highlands.

Mare Imbrium is the largest of the dark plains that dominate the side of the Moon facing Earth. Several high mountains and lighter colored highlands strewn with craters ring Mare Imbrium. (*Carnegie Observatories*)



**Figure 36.5** Mare basalt.

This 1.5-kg specimen of mare basalt was returned to Earth by the *Apollo 15* astronauts in 1971. The small holes covering about a third of the surface are a result of gas dissolved under pressure in the lava from which the rock solidified. Bubbles formed when the lava reached the airless lunar surface, and some of them were frozen in place as the rock cooled. (*NASA*)



**Figure 36.6** Impact breccias.

Impact breccias are created from shattered debris fused under high temperature and pressure. Such conditions prevailed immediately following large impacts on the Moon's surface. (NASA)

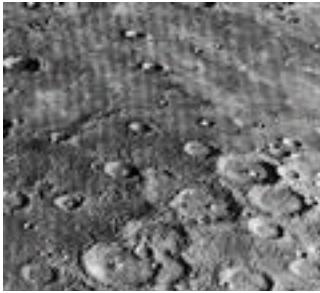


**Figure 36.7** Mercury's craters and plains.

*Mariner 10* took this photograph of Mercury's northern hemisphere in 1974. The broad plains marked with many craters cover an area 480 km wide in this photo. (NASA)

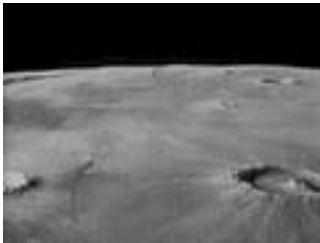


**Figure 36.8** Computer simulation of formation of a scarp on Mercury.

Mercury has numerous long cliffs, or scarps, which are believed to have formed as the planet cooled. As Mercury's mantle and molten iron core cooled and contracted, its crust wrinkled and formed scarps. (NASA)



**Figure 36.9** Mercury and our Moon.

Mercury (left) and Earth's Moon (right) are shown here at the same scale. Both the Moon and Mercury have heavily cratered surfaces and virtually no atmosphere. Mercury, however, has broad plains separating many craters, whereas lunar craters are densely packed, with one overlapping the next. (NASA/Lick Observatory)



**Figure 36.10** Venus's cloud cover.

Ultraviolet image of Venus's clouds from the *Pioneer Venus Orbiter*. Seen in visible light, the clouds are almost featureless. Reflected ultraviolet light reveals their structure and patterns. The thick cloud cover traps heat from the Sun, creating an extreme greenhouse effect. These clouds circle Venus in about 4 days, much faster than the 243-day rotation period of Venus itself, indicating that the atmosphere is in high-speed motion. Although they resemble Earth's clouds, Venus's clouds are not made of water droplets. They are very dry and are composed of droplets of sulfuric acid. (NASA/JPL)

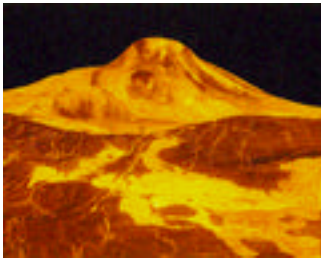


**Figure 36.11** Maat Mons, Venus's highest volcano.

Maat Mons, the highest volcano on Venus is 8 km high. Lava flows extend for hundreds of kilometers across the fractured plains shown in the foreground. Some scientists speculate that Maat Mons might be an active volcano. In this three-dimensional perspective view, simulated (false) color and a digital elevation map developed by the U.S. Geological Survey are used to enhance small-scale structure. The orange color is based on color images recorded by the Soviet *Venera* spacecraft that indicated the surface has a very slight orange tint. The Synthetic Aperture Radar (SAR) data used to make this image shows rough areas as brighter oranges and smooth areas as darker colors. (NASA/JPL)



**Figure 36.12** Pancake domes on Venus.

This cluster of four overlapping pancake domes is located on the eastern edge of Alpha Regio. The domes average about 25 km in diameter with maximum heights of 750 m. These features can be interpreted as viscous or thick eruptions of lava coming from a vent on the relatively level ground, allowing the lava to flow in an even lateral pattern. (NASA/JPL)

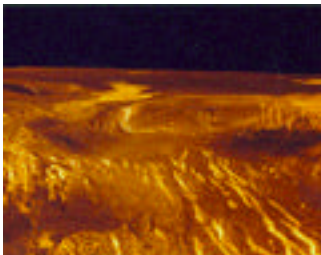


**Figure 36.13** Corona on Venus.

Computer-simulated view of a corona on the surface of Venus. The viewpoint is located 150 km north of Gula Mons at a height of 1.6 km above the corona. This corona has a diameter of 97 km, although coronae on Venus range up to 2000 km in diameter. Coronae appear to be the result of a mantle plume that became inactive before it could form a true shield volcano. (NASA/JPL)

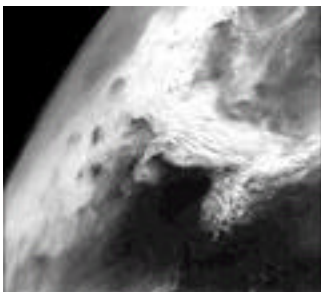


**Figure 36.14** Dust storm on Mars.

This *Viking 2 Orbiter* image shows a large dust storm over the Thaumasia region on Mars. This large disturbance grew into the first global dust storm observed by the *Viking Orbiter*. This image was taken near perihelion (closest approach of Mars to the Sun), when heating of Mars is at a maximum. Dust storms are common during perihelion, when the planet receives 40 percent more sunlight than during aphelion (when Mars is farthest from the Sun). This annual variation in sunlight results in a 20°C increase in temperature during perihelion. The increased temperature causes continental-scale dust storms at the planet's surface. The dust is swept aloft to altitudes of tens of kilometers, where it spreads globally, absorbs light from the Sun, and heats the entire atmosphere by about another 15°-28°C. Mars also has a distinctive

aphelion climate. The cold atmospheric conditions during aphelion stimulate the formation of planetwide belts of water ice clouds surrounding the planet at altitudes of 3 to 10 km. Surface dust raised by low dust storms is confined to low altitudes (about 10 km) and is eventually swept to the ground by the water ice clouds. The clouds further reduce atmospheric temperatures by forming around the dust. Without sunlight, the dust freezes and falls to the ground. This strong competition between dust heating and cloud cooling drives sweeping annual and short-term regional changes in Mars's climate. (NASA/JPL)



**Figure 36.15** Olympus Mons. (a) Overhead view; (b) perspective view.

(a) Olympus Mons, the largest volcano in the solar system, is a shield volcano, similar to volcanoes in Hawaii. The central edifice of Olympus Mons has a summit caldera 24 km above the surrounding plains. Surrounding the volcano is an outward-facing scarp 550 km in diameter and up to 6 km high in places. In other places, it is hidden under lava flows cascading out into the surrounding lava plains. This cliff is unique among the giant shield volcanoes on Mars. Beyond the scarp is a moat filled with lava, most likely derived from Olympus Mons. The rough, crinkly areas around Olympus Mons form the Olympus Mons Aureole. Both the Aureole and the basal cliff are poorly understood, but their origins may be related: one theory holds that the basal cliff was formed by many large landslides and that the Aureole marks material piled up at the bottom of these landslides. (NASA/JPL)



(b) Perspective view of Olympus Mons created from several images taken from different spacecraft positions and combined with a computer model of the surface topography. The final mosaic shows the volcano as it would be seen from the northeast. The basal cliff and gentle rolling slopes higher up the volcano are clearly visible. The faint radial texture above the basal cliff marks the traces of thousands of separate lava flows. Places where lavas have flowed over the basal cliff can be seen to the left and at lower right. (NASA/JPL)

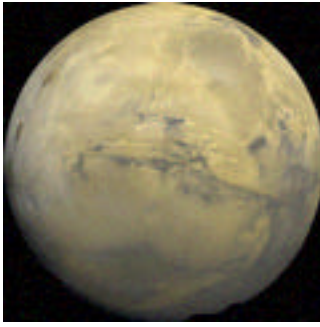


**Figure 36.16** Valles Marineris hemisphere of Mars.

Mosaic, composed of 102 *Viking Orbiter* images, of the Valles Marineris hemisphere of Mars projected into point perspective, a view similar to what one would see from a spacecraft. The viewer's distance is 2500 km from the surface of the planet. The center of the photo shows the entire Valles Marineris canyon system, over 3000 km long and up to 8 km deep and 200 km wide in places. Several of Earth's Grand Canyons—446 km long, 30 km wide, and 1.6 km deep—would fit into the mammoth Valles Marineris. The structure extends from Noctis Labyrinthus, the arcuate system of graben to the west, to the chaotic terrain to the east. Many huge ancient river channels begin from the chaotic terrain and north-central canyons and run north. A number of the channels flowed into a basin called Acidalia Planitia, which is the dark area in the extreme north of this picture. South of Valles Marineris is very ancient terrain covered by many impact craters. (NASA/JPL)



**Figure 36.17** Ancient river channels on Mars.

The existence of braided riverbeds on Mars suggests that the planet's atmosphere was thicker and its climate more Earthlike long ago, when liquid water flowed across its surface. Any water exposed to the sparse Martian atmosphere today would rapidly boil away or freeze solid. (NASA)

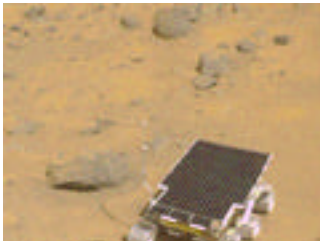


**Figure 36.18** Sojourner, the *Pathfinder* rover, on the surface of Mars.

This image shows Sojourner as it left the rear ramp of Sagan Memorial Station (the lander). (NASA)



**Figure 36.19** Mars's twin moons. (a) Phobos; (b) Deimos.

(a) *Viking* image of Phobos, Mars's larger moon. (NASA)

(b) *Viking* image of Deimos, Mars's smaller moon. (NASA)



**Figure 36.20** Jupiter.

This processed color image of Jupiter was produced in 1990 by the U.S. Geological Survey from a 1979 *Voyager* image. The colors have been enhanced to bring out detail. Zones of light-colored, ascending clouds alternate with bands of dark, descending clouds. The clouds travel around the planet in alternating eastward and westward belts at high speeds. Tremendous storms as big as Earthly continents surge around the planet. The Great Red Spot (oval shape toward the lower left) is an enormous storm that drifts along its belt, eventually circling the entire planet. (NASA/USGS)

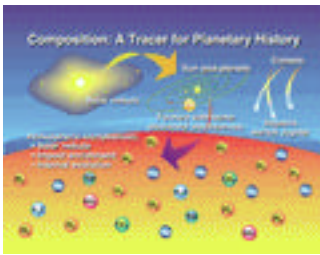


**Figure 36.21** Processes contributing to Jupiter's atmospheric composition.

Jupiter's strong gravity trapped a sample of all the ingredients in the solar nebula from which the Sun and planets formed 4.5 billion years ago. From Jupiter's size and mass, astronomers have long known that it is made almost entirely of hydrogen and helium, the two most abundant elements in the Sun and in the universe as a whole. Planetesimals formed from the solar nebula and became the building blocks of the planets. Collisions between these icy planetesimals are believed to have produced a large icy core onto which hydrogen and helium gas was trapped to form Jupiter. Planetesimals remaining after the formation of the planets have bombarded Jupiter (as well as the other planets) during the past 4.5 billion years. These small bodies have enriched the mainly hydrogen and helium gas of Jupiter's atmosphere with heavier elements—mainly carbon (in the form of methane,  $\text{CH}_4$ ), nitrogen (in the form of ammonia,  $\text{NH}_3$ ), oxygen (in the form of water,  $\text{H}_2\text{O}$ ), and sulfur (in the form of hydrogen sulfide,  $\text{H}_2\text{S}$ ). By determining the abundances of these gases, additional information can be obtained about the planetary formation process and the role of impacts in planetary evolution. (NASA/Ames)

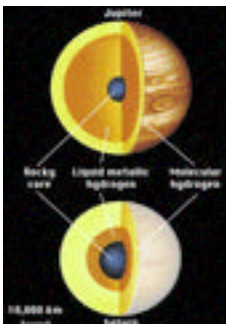


**Figure 36.22** Interior structures of Jupiter and Saturn.

The interiors of both Jupiter and Saturn are believed to have three regions: a rocky core, a metallic hydrogen shell, and a layer of molecular hydrogen. Saturn's rocky core is larger than Jupiter's, and it has a much smaller liquid metallic hydrogen mantle. (From Kaufmann and Comins, *Discovering the Universe, 4th ed.*)

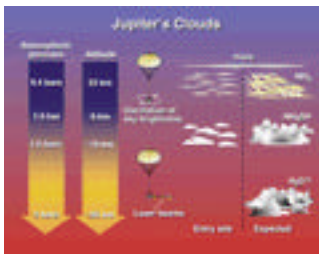


**Figure 36.23** Summary of *Galileo* probe results on Jupiter's clouds.

Two experiments on the probe detected clouds using different techniques. One experiment, based on oscillation of sky brightness, detected a cloud layer near the 0.6-bar pressure level. Based on its location, this cloud layer is believed to be composed of ammonia ice particles. The other experiment, based on observing scattered laser light from cloud particles, found one well-defined, tenuous cloud structure with a base at the 1.6-bar pressure level, as well as faint traces of cloud particles at a wide range of altitudes. No other cloud layers were found—in particular, the one cloud layer detected by the first experiment was not seen. The simplest explanation for this apparent contradiction between the experiments is that the upper cloud layer near 0.6 bar is patchy and the probe went through a clear area.

The profound difference between the entry site's cloud structure and the cloud structure expected for "average" Jupiter is illustrated at right. The "expected" picture is based on theoretical modeling and interpretation of Earth-based and spacecraft-based observations of large regions of Jupiter. Layers of ammonia, ammonium hydrosulfide, and water clouds were predicted. However, no thick, dense clouds were found, and no water cloud was detected. The entry of the *Galileo* probe into an infrared "hot spot" may account for most, if not all, of the deviations from expectations, because "hot spots" are believed to represent regions of reduced cloud cover and are not common on Jupiter. (NASA/Ames)

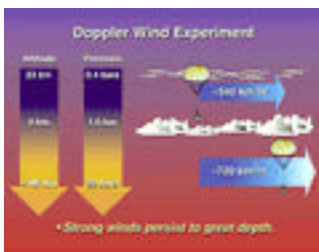


**Figure 36.24** *Galileo* probe wind experiment.

Illustration of the variation with depth of the strong eastward winds at the probe entry site. As seen in this figure, winds just below the cloud tops were found to be as strong as the strongest winds observed by the Hubble Space Telescope at this site. These strong winds persisted and even increased with depth until the end of the probe's radio transmissions. Previous studies of Jupiter's cloud-top motions have shown a very unusual wind system consisting of strong eastward and westward jet streams alternating with latitude, quite unlike Earth's wind system. The *Galileo* probe's observations have now provided the third dimension to the winds at one location and show that the wind system at the probe entry site is deep. Initial interpretation of these observations suggests that Jupiter's internal heat source, rather than heating by sunlight, plays the major role in generating the observed winds. Further theoretical work and computer simulations are needed, however, to understand this important observa-

tion by the *Galileo* probe fully. (NASA/Ames)

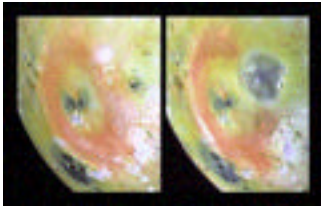


**Figure 36.25** Surface changes on Io.

These images show dramatic changes on Io's surface during a five-month period. *Galileo* captured the left frame during its seventh orbit of Jupiter, the right frame during its tenth orbit. A new dark spot, 400 km in diameter (roughly the size of Arizona), surrounds a volcanic center named Pillan Patera. *Galileo* imaged a 120-km-high plume erupting from this location during its ninth orbit. Pele, which produced the larger plume deposit southwest of Pillan, also appears different than it did during the seventh orbit, perhaps as a result of interaction between the two large plumes. (NASA/JPL)

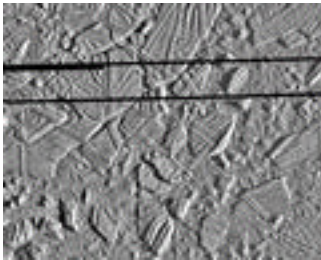


**Figure 36.26** Europa ice rafts.

This high-resolution image taken by *Galileo* on February 20, 1997, shows the ice-rich crust of Europa. Seen here are crustal plates ranging up to 13 km across, which have been broken apart and "rafted" into new positions, superficially resembling the disruption of pack-ice on polar seas during spring thaws on Earth. The size and geometry of these features suggest that motion was enabled by ice-crustated water or soft ice close to the surface at the time of disruption. (NASA/JPL)

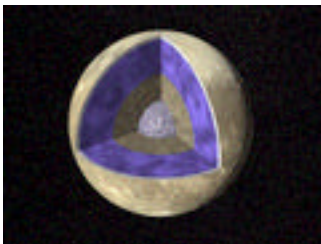


**Figure 36.27** Interior of Ganymede.

*Voyager* images were used to create a global view of Ganymede. The cutout reveals the four-layer interior structure, based on measurements of Ganymede's gravity field and theoretical analyses using Ganymede's known mass, size, and density. Ganymede's surface is rich in water ice, and *Voyager* and *Galileo* images show features that are evidence of geological and tectonic disruption of the surface in the past. These geological features reflect forces and processes deep within Ganymede's interior. Based on geochemical and geophysical models, scientists expected Ganymede's interior to consist of either an undifferentiated mixture of rock and ice or a differentiated structure with a large Moon-sized core of rock and possibly iron, overlain by a deep layer of warm, soft ice and capped by a thin, cold, rigid ice crust. *Galileo*'s measurements of Ganymede's gravity field have basically confirmed the differentiated model and allowed scientists to estimate the size of these layers more accurately. In addition, the data strongly suggest a dense metallic core at the center of the rock core. This metallic core implies a greater degree of heating at some time in Ganymede's past than had been proposed before

and may be the source of Ganymede's magnetic field, which was discovered by *Galileo*'s space physics experiments. (NASA/JPL)



**Figure 36.28** Saturn and six of its moons.

This montage of images of the Saturn system was prepared from an assemblage of images taken by the *Voyager 1* spacecraft during its Saturn encounter in November 1980. Dione is in the foreground, Saturn is rising behind, Tethys and Mimas are fading in the distance to the right, Enceladus and Rhea are off Saturn's rings to the left, and Titan is in its distant orbit at the top. (NASA/JPL)

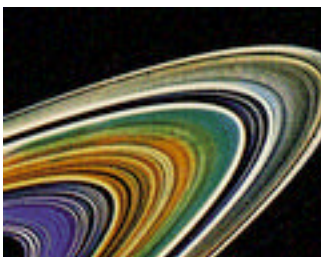


**Figure 36.29** Saturn's rings.

Details of Saturn's rings are visible in this *Voyager 2* photograph. The rings are actually composed of thousands of closely spaced ringlets. The colors are exaggerated by computer processing to show the ringlets more clearly. (NASA/JPL)

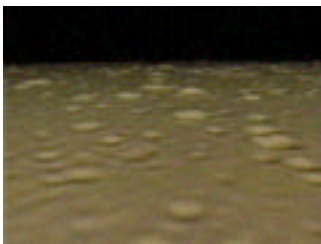


**Figure 36.30** Computer-simulated flight over Enceladus.

This computer-simulated flight over Enceladus is based on images from *Voyager 2*. Ice flows and cracks strongly suggest that the surface of Enceladus has been geologically active recently, perhaps as a result of heating by tidal forces. (NASA)



**Figure 36.31** Uranus and its moons.

Montage of images of the Uranian system prepared from an assemblage of images taken by *Voyager 2* during its Uranus encounter in January 1986. Ariel is in the foreground, with Uranus rising behind it; Umbriel is off to the left; Miranda is in the right foreground; Titania is in the distance at the far right; and Oberon is in its distant orbit at the top. (NASA/JPL)

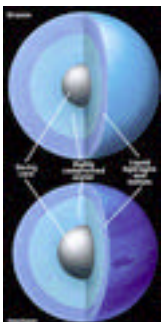


**Figure 36.32** Interior structures of Uranus and Neptune.

The interiors of Uranus and Neptune are thought to consist of a rocky core, surrounded by a compressed liquid water mantle, which is in turn surrounded by a layer of liquid hydrogen and helium. (From Kaufmann and Comins, *Discovering the Universe*, 4th ed.)

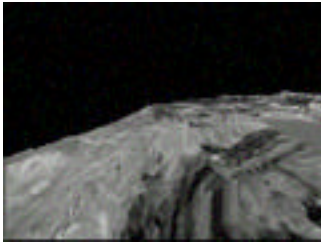


**Figure 36.33** Computer-simulated flight over Miranda.

This simulated flight over the bizarre surface of Miranda was constructed from *Voyager 2* images. Scientists don't yet have a good explanation for the jumbled, haphazard terrain of canyons, terraces, and younger and older surfaces. (NASA)

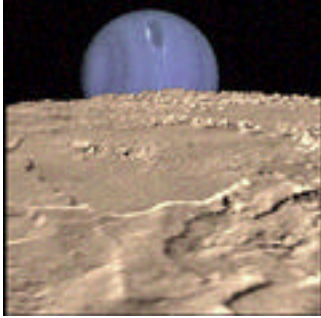


**Figure 36.34** A view of Neptune from Triton.

Composite view created from *Voyager* images showing Neptune on Triton's horizon. Neptune's south pole is to the left. Clearly visible in the southern hemisphere is the Great Dark Spot, a large storm system that disappeared in 1994. The foreground is a computer-generated view of Triton's maria as they would appear from a point approximately 45 km above the surface. The terraces visible in this image indicate multiple episodes of cryovolcanic flooding. Neptune is neither rising nor setting in this image. Because of Triton's motion relative to Neptune, it would appear to move laterally along the horizon, eventually rising and setting at high latitudes. (NASA/JPL)



**Figure 36.35** Computer-simulated flight over Triton.

This large moon may once have been captured by Neptune's gravitation, and much of its surface covered with ice. Notice the sparse craters.



**Figure 36.36** Pluto and Charon.

This is the clearest view yet of the distant planet Pluto and its moon, Charon, as revealed by NASA's Hubble Space Telescope (HST). The Hubble observations show that Charon is bluer than Pluto. This means that the worlds have different surface composition and structure. A bright highlight on Pluto suggests that it has a smoothly reflecting surface layer. (Dr. R. Albrecht, ESA/ESO Space Telescope European Coordinating Facility; NASA)